

# Data-driven discoveries of Bäcklund transforms and soliton evolution equations via deep neural networks learning

Zijian Zhou<sup>1,2</sup>, Li Wang<sup>3,4</sup>, Weifang Weng<sup>1,2</sup>, and Zhenya Yan<sup>1,2,\*</sup>

<sup>1</sup>*Key Laboratory of Mathematics Mechanization, Academy of Mathematics and Systems Science, Chinese Academy of Sciences, Beijing 100190, China*

<sup>2</sup>*School of Mathematical Sciences, University of Chinese Academy of Sciences, Beijing 100049, China*

<sup>3</sup>*Yanqi Lake Beijing Institute of Mathematical Sciences and Applications, Beijing, 101408, China*

<sup>4</sup>*Yau Mathematical Sciences Center and Department of Mathematics, Tsinghua University, Beijing, 100084, China*

**Abstract** We introduce a deep neural network learning scheme to discover the Bäcklund transforms (BTs) of soliton evolution equations and an enhanced deep learning scheme for data-driven soliton equation discovery, respectively. The first deep learning scheme takes advantage of some solution (or soliton equation) informations to train the data-driven BT discovery, and is valid in the study of the BT of the sine-Gordon equation, and complex and real Miura transforms between the defocusing (focusing) mKdV equation and KdV equation, as well as the data-driven mKdV equation discovery via the Miura transforms. The second deep learning scheme uses the higher-order solitons generated by the explicit/implicit BTs to study the data-driven discoveries of mKdV and sine-Gordon equations, in which the high-order soliton informations are more powerful for the enhanced leaning soliton equations with higher accuracies.

**Keywords** Soliton equations; Bäcklund transforms; Solitons; Deep neural networks learning; Data-driven inverse problems

## 1 Introduction

In the fields of applied mathematics and nonlinear mathematical physics, there are many types of physically interesting nonlinear evolution partial differential equations (PDEs). Particularly, since the well-known Korteweg-de Vries (KdV) equation with solitary waves was presented by Korteweg and de Vries [1], various of soliton evolution equations (e.g., the Boussinesq equation, mKdV equation, KP equation, sine-Gordon equation, nonlinear Schrödinger equation, Gross-Pitaevskii equation) [2] play the important roles in the fields of nonlinear science, such as fluid mechanics, nonlinear optics, quantum optics, Bose-Einstein condensates, plasmas physics, ocean, atmosphere, biology, and even finance [3–9]. Many types of analytical, numerical and experimental approaches have been used to deeply explore the wave structures and properties of these soliton equations (see, e.g., Refs. [2–8, 10] and references therein).

Since Bäcklund [11] first found a transform (alias the auto-Bäcklund transform (aBT)) of the sine-Gordon equation  $u_{xt} = \sin u$  in 1875, and Darboux [12] found a transform (alias Darboux transform) of the Sturm-Liouville equation (alias the linear Schrödinger equation)  $\psi_{xx} + [\lambda - V(x)]\psi = 0$  in 1882, many types of well-known analytical transforms were found between the same equation or different equations [13–18]. For example, Hopf [19] and Cole [20] independently established a BT between the nonlinear Burgers equation  $u_t + uu_x - \mu u_{xx}$  and linear heat (or diffusion) equation  $v_t - \mu v_{xx} = 0$  in 1950-1951. In 1967, Gardner, Greene, Kruskal, and Miura (GGKM) [21] solved the initial value problem of the KdV equation starting from its coupled linear PDEs, which are just its Lax pair [2]. In 1968, strongly motivated by the GGKM's idea, Lax [22] presented a general formal BT (alias Lax pair) implying that the eigenvalues of the linear operator  $\{L(\phi)\psi = \lambda\psi(\phi), \psi_t = B(\phi)\psi\}$  are integrals of the nonlinear equation  $\phi_t = K(\phi)$ . In the same year, Miura [23] found a new BT (alias the

---

\* *Email address:* zyyan@mmrc.iss.ac.cn (Corresponding author)

Miura transform (MT)) between the KdV equation  $v_t + 6vv_x + v_{xxx} = 0$  and focusing (or defocusing) mKdV equation  $u_t \pm 6u^2u_x + u_{xxx} = 0$ .

With the quick development of cloud computing resources and mass data, deep learning [24, 25] has been used in many fields containing cognitive science [26], image recognition [27], genomics [28], industrial areas [29, 30], and etc. In particular, in the past of decades, some deep neural network learning methods [31–39] have been developed to study the partial differential equations (PDEs), which play an important role in the various of scientific fields. The powerful physics-informed neural network (PINN) method [38, 39] was used to investigate the PDEs [40–48], the fractional PDEs [49], and stochastic PDEs [50].

In this paper, we would like to develop two kinds of deep neural network learning methods to study the data-driven discoveries of BTs and soliton equations via the general system

$$\begin{cases} F(u, u_t, u_x, u_{tt}, u_{tx}, u_{xx}, \dots) = 0, & (1a) \\ G(u', u'_t, u'_x, u'_{tt}, u'_{tx}, u'_{xx}, \dots) = 0, & (1b) \\ \phi_i(u, u_t, u_x, u_{tt}, u_{tx}, u_{xx}, \dots, u', u'_t, u'_x, u'_{tt}, u'_{tx}, u'_{xx}, \dots) = 0, \quad (i = 1, 2, \dots), & (1c) \end{cases}$$

where  $u = u(x, t)$ ,  $u' = u'(x, t)$ , the considered spatio-temporal region is  $(x, t) \in [-L, L] \times [-T, T]$ , Eq. (1c) is called the BT between Eqs. (1a) and (1b). In particular, if Eq. (1b) is equivalent to Eq. (1a), then the transform (1c) is called the aBT. It is obvious to see that the information of Eq. (1a) can be shifted to Eq. (1b) with the aid of BT (1c). Sometimes, the structure of the transformed Eq. (1b) may become simpler. Therefore, BTs can be used to discover the new informations between Eqs. (1a) and (1b).

The rest of this paper is organized as follows. In Sec. 2, we will introduce a deep neural network learning scheme to study aBTs and BTs, e.g., the aBT of the sine-Gordon equation, and Miura transform between the focusing/defocusing mKdV equation and KdV equation. Moreover, the deep learning scheme can also be used to discover soliton equations with the aid of BTs. In Sec. 3, a new deep learning method discovering the soliton equations is displayed based on the BTs. We use the implicit and explicit BTs to exhibit the data-driven discoveries of the sine-Gordon equation and mKdV equation with the aid of the aBT of the sine-Gordon equation, and Darboux transform of the focusing mKdV equation, respectively. Finally, some conclusions and discussions are summarized in Sec. 4.

## 2 Data-driven discoveries of BTs and soliton equations

### 2.1 Deep learning scheme discovering the BTs and equations via BTs

We here would like to introduce the deep learning scheme for the discoveries of BTs and soliton equations by examining system (1). The main idea of this scheme is to use some constraints on  $u(x, t)$  and  $u'(x, t)$  to find the approximate transform between  $u(x, t)$  and  $u'(x, t)$ , where  $u(x, t)$  and  $u'(x, t)$  are represented by one or two deep neural networks. There are many kinds of neural networks including the fully-connected neural network, convolution neural network, and recurrent neural network. The constraints of the functions include the real solution data-set and the corresponding equations. The aim of the scheme is to make the neural network solution approach to the real data better and match some physical laws efficiently.

Figure 1 displays the deep learning scheme of the BT discovery, where  $u(x, t)$  and  $u'(x, t)$  are represented by a deep neural network, which is, in general, chosen as a fully-connected neural network. It will share the same network parameters, weights, and biases. For some conditions, they can be represented by two different networks to eliminate mutual influence. In this diagram, we assume that  $u(x, t)$  and  $u'(x, t)$  are real-valued functions. If the solutions of Eq. (1a) are complex, the number of output neurons would be double. The number of input neurons equals to the independent variables of  $u(x, t)$  and  $u'(x, t)$ .  $\tau$  represents the activation function, and is chosen as  $\tau(x) = \tanh(x)$  in this scheme, whose aim is to add the nonlinear action to the

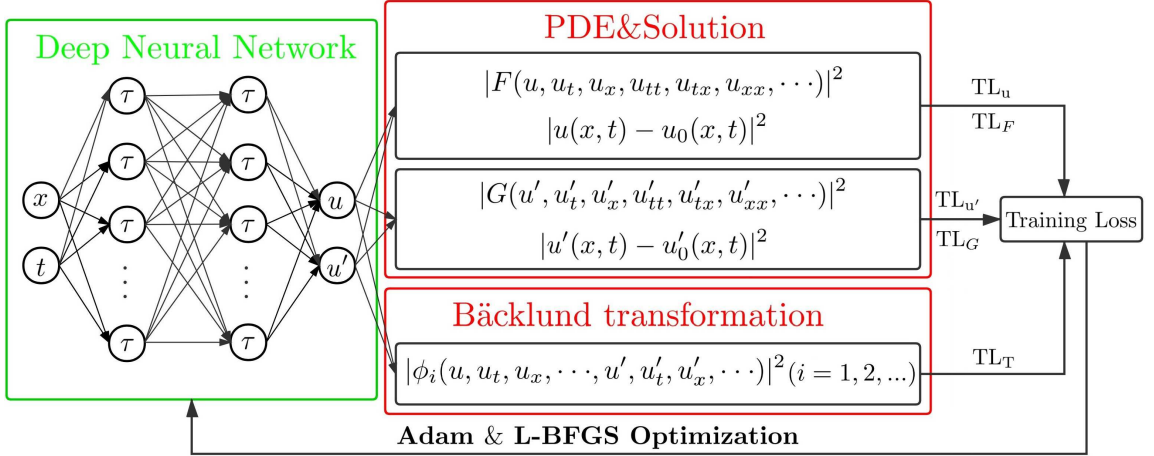


Figure 1: The deep learning scheme for the data-driven discovery of BTs and soliton equations.

deep neural network. Notice that one can also choose other types of activation functions, such as the sigmoid (logistic) function, threshold function, piecewise linear function, ReLU function, ELU function, swish function, and softmax function [45].

The loss function during the training process consists of three different parts. It can be simply written as:

$$\text{TL} = \text{TL}_T + \text{TL}_{F/u} + \text{TL}_{G/u'}, \quad (2)$$

which can be called T-part ( $\text{TL}_T$ ), F-part ( $\text{TL}_{F/u}$ ), and G-part ( $\text{TL}_{G/u'}$ ), and are defined by

$$\begin{aligned} \text{TL}_F &= \frac{1}{N_p} \sum_{j=1}^{N_p} |F(u(x_j, t_j), u_t(x_j, t_j), u_x(x_j, t_j), \dots)|^2, \\ \text{TL}_u &= \frac{1}{N_p} \sum_{j=1}^{N_p} |u(x_j, t_j) - u_0(x_j, t_j)|^2, \\ \text{TL}_G &= \frac{1}{N_p} \sum_{j=1}^{N_p} |G(u'(x_j, t_j), u'_t(x_j, t_j), u'_x(x_j, t_j), \dots)|^2, \\ \text{TL}_{u'} &= \frac{1}{N_p} \sum_{j=1}^{N_p} |u'(x_j, t_j) - u'_0(x_j, t_j)|^2, \\ \text{TL}_T &= \frac{1}{N_p} \sum_{j=1}^{N_p} |\phi_j(u, u_t, u_x, \dots, u', u'_t, u'_x, \dots)|^2_{(x,t)=(x_j,t_j)}, \end{aligned} \quad (3)$$

where  $\{x_j, t_j\}_{j=1}^{N_p}$  denote the set of sampling points in some spatio-temporal region  $(x, t) \in [-L, L] \times [-T, T]$ ,  $N_p$  stands for the number of sampling points, which are generated by using the Latin Hypercube Sampling strategy [51], and  $\{u_0(x_j, t_j)\}_{j=1}^{N_p}$  and  $\{u'_0(x_j, t_j)\}_{j=1}^{N_p}$  represent the sampling solution data of Eqs. (1a) and (1b), respectively.

The data type determines the selection of the loss function. To make the neural network satisfy the structures of the equations and BTs, the loss function should contain the above three parts. Specifically, if we assume

that the discovery problem of BTs contains both data sets,  $\{u_0(x_j, t_j)\}_{j=1}^{N_p}$  and  $\{u'_0(x_j, t_j)\}_{j=1}^{N_p}$ , then all terms of the loss function (3) can be added to the final loss function (2). This case is displayed in the subsection 2.2.2. But if it only contains one data-set, the algorithm also works when the equation loss ( $TL_F$  or  $TL_G$ ) of missing data-set function is added to the final loss function. For instance, the only data-set  $\{u_0(x_j, t_j)\}_{j=1}^{N_p}$  is known in the following subsection 2.2.1 about the BT discovery of the sine-Gordon equation.

Based on this framework, we can also study another question: learning the equation from the data-set of another equation by a BT. Generally speaking, if the BT is explicit, then the given data-set can be easily transformed into the data-set of another unknown function. But if the BT is implicit, it is not easy to study this question (without loss of generality, we assume that  $u'_0(x, t)$  is implicit with respect to  $u_0(x, t)$ ). In our framework, although the BT is implicit, the T-part loss function can convert the data-set of  $u_0(x, t)$  to the data-set of  $u'_0(x, t)$ . The estimated data-set of  $u'_0(x, t)$  will be represented as the neural network approximated solution, and the loss function  $TL_G$  will be used to train the unknown parameters in the equation  $G = 0$  to approach the right values. The subsection 2.3 will verify the effectiveness of our framework in terms of some examples.

In the scheme, firstly, for a set of larger sampling points, we would like to use an efficient mini-batch optimization algorithm Adam [52]. Secondly, the model will be trained by a full-batch optimization algorithm L-BFGS [53] until the difference of the loss function is less than the Machine Epsilon. In what follows, we will use some examples to verify the validity of our deep learning scheme.

## 2.2 Examples of the data-driven BT/MT discoveries

In what follows, we would like to use the known equations (e.g., sine-Gordon equation (4), the focusing mKdV equation (11) with the KdV equation (13), or defocusing mKdV equation (12) with the KdV equation (13)) and their corresponding known solution (8), (16) with (17), or (20) with (21) to discover the unknown BT (6), the complex Miura transform (14), or real Miura transform (18) by using the above deep learning scheme, respectively.

### 2.2.1 Data-driven BT discovery of the sine-Gordon equation

The well-known sine-Gordon (s-G) equation [54]

$$u_{xt} = \sin u, \quad u(x, t) \in \mathbb{R}[x, t] \quad (4)$$

is a physically interesting model, and can be used to describe the theory of crystal dislocations, Bloch-wall motion, splay waves in lipid membranes, magnetic flux on a Josephson line, and elementary particles [55–57]. The s-G equation (4) admits the auto-Bäcklund transform (aBT) [11]

$$\begin{cases} u'_x = u_x - 2\beta \sin\left(\frac{u+u'}{2}\right), \\ u'_t = -u_t + \frac{2}{\beta} \sin\left(\frac{u-u'}{2}\right), \end{cases} \quad (5)$$

where  $\beta \neq 0$  is an arbitrary real-valued constant, that is, if  $u(x, t)$  is a solution of the s-G equation (4), then so is  $u'(x, t)$  given by Eq. (5). In what follows, we would like to use the above-mentioned deep learning method to discover the parameters of the aBT (5). For convenience, we consider the generalized aBT

$$\begin{cases} u'_x = au_x - b \sin\left(\frac{u+u'}{2}\right) + hu_x, \\ u'_t = -cu_t + d \sin\left(\frac{u-u'}{2}\right) - fu_t, \end{cases} \quad (6)$$

where the parameters  $a, b, c, d, h,$  and  $f$  are real-valued parameters to be determined later, the two new quadratic nonlinear terms are introduced in the unknown aBT (6). In particular, as  $a = c = 1, b = 2\beta, d = 2/\beta, h = f = 0,$  the unknown aBT (6) reduces to the known exact aBT (5).

We use the above-mentioned deep leaning scheme to discover the aBT of the s-G equation in two cases by considering the system

$$\begin{cases} u'_{xt} - \sin u' = 0, \\ u'_x - au_x + b \sin\left(\frac{u+u'}{2}\right) - huu_x = 0, \\ u'_t + cu_t - d \sin\left(\frac{u-u'}{2}\right) + fuu_t = 0 \end{cases} \quad (7)$$

in the spatio-temporal region  $(x, t) \in [-10, 10] \times [-5, 5],$  where  $a, b, c, d, h,$  and  $f$  are parameters to be determined. The training data are generated by using the breather solution of the s-G equation (4) [56]

$$u = 4 \arctan\left(\frac{\tan(\mu)\sin(X \cos(\mu))}{\cosh(T \sin(\mu))}\right), \quad X = \frac{(1-k)x - (1+k)t}{\sqrt{1-k^2}}, \quad T = \frac{(1-k)x + (1+k)t - x_0}{\sqrt{1-k^2}}, \quad (8)$$

where  $k \in [0, 1), \mu \neq 0.$  The breather solution data-set  $(TL_u)$  given by Eq. (8) and original equation  $(TL_f)$  given by Eq. (4) together generate the F-part loss. The undetermined transforms form the T-part loss. And the G-part loss is only formed by the transformed equation  $(TL_f).$

Here, the hidden neural network  $\hat{u}(x, t)$  in Python can be defined as

```
def u(x, t):
    U = neural_net(tf.concat([x, t], 1), weights, biases)
    u = U[:, 0:1]
    v = U[:, 1:2]
    return u, v
```

such that the residual neural network  $f_{sG}(x, t)$  and  $f_{BT}(x, t)$  in Python can be obtained as

```
def f_sG(x, t):
    u, v = u(x, t)
    v_t = tf.gradients(v, t)[0]
    v_x = tf.gradients(v, x)[0]
    v_xt = tf.gradients(v_x, t)[0]
    u_x = tf.gradients(u, x)[0]
    u_t = tf.gradients(u, t)[0]
    f_sG = v_xt - sin(v)
    f_BT1 = v_x - a * u_x + b * tf.sin((u + v) / 2) - h * u * u_x
    f_BT2 = v_t + c * u_t - d * tf.sin((u - v) / 2) + f * u * u_t
    return f_sG, f_BT1, f_BT2
```

*Case A.*—In this case, we suppose that  $a, b, c,$  and  $d$  are unknown parameters, and  $h = f = 0.$  It should be pointed out that the two parameters  $b$  and  $d$  are not fixed. We know that  $bd = 4$  in the given exact aBT (5) such that we only consider the product value of  $b$  and  $d$  in the deep learning. We use a 6-layer neural network with 5 hidden layers and 40 neurons per layer to learn system (7). Without loss of generality, we take the initial value of all free parameters as 1, i.e.,  $a = b = c = d = 1.$  We choose  $(x, t) \in [-10, 10] \times [-5, 5]$  as the training region, from which 10,000 sample points are taken by the Latin Hypercube Sampling strategy [51]. Moreover, the 20,000 steps Adam and 50,000 steps L-BFGS optimizations are used in the deep learning. Fig. 2(a) displays the trained breather solution by using the deep neural network. Case A in Table 1 exhibits the learning parameters

Table 1: Data-driven discovery of parameters  $a, bd, c, h, f$  in aBT (6) and errors, as well as training times.

Case	$a$	$b \cdot d$	$c$	$h$	$f$	
Exact	1	4	1	0	0	
A (no noise)	1.00007	4.00006	1.00001	0	0	
A (2% noise)	0.99995	4.00057	1.00003	0	0	
B (no noise)	1.00004	4.00021	1.00001	$-4.24 \times 10^{-7}$	$-2.51 \times 10^{-6}$	
B (2% noise)	0.99988	3.99959	0.99985	$-3.90 \times 10^{-4}$	$-3.60 \times 10^{-4}$	

Case	error of $a$	error of $b \cdot d$	error of $c$	error of $h$	error of $f$	time
A (no noise)	$7.44 \times 10^{-5}$	$6.45 \times 10^{-5}$	$1.31 \times 10^{-5}$	0	0	619.92s
A (2% noise)	$5.29 \times 10^{-4}$	$5.74 \times 10^{-4}$	$3.24 \times 10^{-5}$	0	0	637.08s
B (no noise)	$4.17 \times 10^{-5}$	$2.12 \times 10^{-4}$	$1.37 \times 10^{-5}$	$4.24 \times 10^{-7}$	$2.51 \times 10^{-6}$	659.96s
B (2% noise)	$1.20 \times 10^{-4}$	$4.05 \times 10^{-4}$	$1.47 \times 10^{-4}$	$3.94 \times 10^{-4}$	$3.57 \times 10^{-4}$	697.76s

about  $a, c, b$  and  $d$ , and their errors under two senses of the training data without a noise and with a 2% noise, respectively, which imply that the used deep learning method is effective. Moreover, the errors are exhibited in Figs. 2(b1, b2) for the cases without a noise and with a 2% noise, respectively. The training times are 619.92s and 637.08s, respectively.

*Case B.*—In this case, we suppose that  $a, b, c, d, h$ , and  $f$  are all unknown parameters. We used the same deep neural network method as Case A to study this case. Case B in Table 1 displays the learning parameters about  $a, b, c, d, h$ , and  $f$ , and their errors under two senses of the training data without a noise and with a 2% noise, respectively, which imply that the used deep learning method is effective. Moreover, the errors are exhibited in Figs. 2(b3, b4) for the cases without a noise and with a 2% noise, respectively. The training times are 659.96s and 697.76s, respectively.

### 2.2.2 Data-driven discovery of Miura transforms

In 1968, Miura [23] presented the well-known complex Miura transform (a special BT)

$$v = iu_x + u^2, \quad i = \sqrt{-1}, \quad (9)$$

and real Miura transform

$$v = u_x - u^2 \quad (10)$$

to transform, respectively, the focusing mKdV equation [2, 23]

$$u_t + 6u^2u_x + u_{xxx} = 0 \quad (11)$$

and the defocusing mKdV equation [2, 23]

$$u_t - 6u^2u_x + u_{xxx} = 0 \quad (12)$$

into the same KdV equation [1]

$$v_t + 6vv_x + v_{xxx} = 0, \quad (13)$$

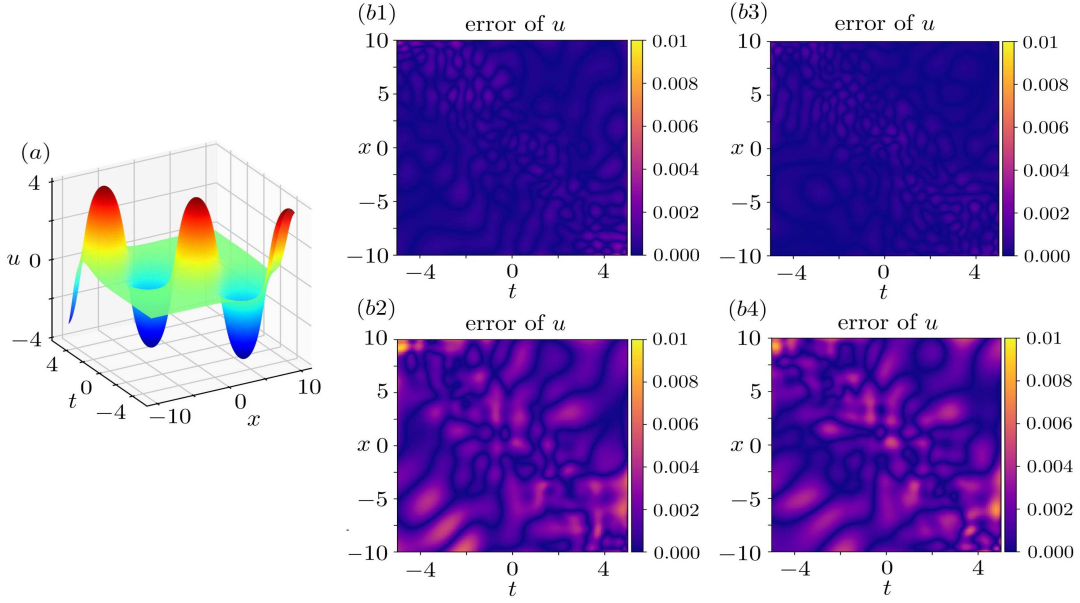


Figure 2: Data-driven aBT discovery of the sine-Gordon equation (4): (a) breather solution (8) generating the training data; (b1-b4) Relative error between exact solution and neural network solution: (b1, b3) training data without a noise; (b2, b4) training data with a 2% noise. The relative  $\mathbb{L}^2$ -norm errors of  $u(x, t)$ , respectively, are (b1)  $3.5255 \cdot 10^{-4}$ , (b2)  $1.3327 \cdot 10^{-3}$ , (b3)  $2.7313 \cdot 10^{-4}$ , and (b4)  $1.3390 \cdot 10^{-3}$ . Training times in (b1-b4) are 619.92s, 659.96s, 637.08s, and 697.76s, respectively.

which can describe the shallow water wave, pressure waves, acoustic waves, magneto-sonic waves, electron plasma waves, and ion acoustic waves [58, 59].

In this subsection, the data-driven deep learning method will be used in two different cases. In the first part, the parameters of Miura transform will be discovered including with and without disturbance terms. The data-set is generated by an exact soliton solution of the mKdV equation and an corresponding exact solution of the KdV equation, which is generated by following soliton solution through the Miura transform. In the second part, an equation will be discovered through the solution of another equation. The data-set is generated by the solution of another equation. The real Miura transform will be used in the T-part loss function to find the unknown equation. In the both cases, the F-part loss is obtained by the exact solution of the mKdV equation given by Eq. (16) or (20) and the original mKdV equation given by Eq. (11) or (12). And the G-part loss is constructed from the exact solution of the KdV equation given by Eq. (17) or (21) and the original KdV equation (13).

### Case 1. Data-driven discovery of the complex Miura transform

In the following, we would like to study the data-driven parameter discovery of the complex Miura transform. We consider the generalized Miura transform

$$v = iau_x + bu^2 + cuu_x + du_{xx}, \quad (14)$$

where  $a, b, c, d$  are four parameters to be determined latter. If  $a = b = 1, c = d = 0$ , then the transform (14) reduces to the known Miura transform (9).

In what follows, we would like to use the above-mentioned deep leaning scheme to discover these parameters  $a, b, c, d$  of the complex Miura transform (14) between the focusing mKdV equation and KdV equation in two

Table 2: Data-driven discovery of the complex Miura transform (14) via system (15):  $a$ ,  $b$ ,  $c$ ,  $d$  and their errors, as well as the training times.

Case	$a$	$b$	$c$	$d$
Exact	1	1	0	0
A (no noise)	0.99931	0.99958	0	0
A (2% noise)	1.00026	0.99981	0	0
B (no noise)	1.00006	0.99990	$-4.1 \times 10^{-4}$	$-1.0 \times 10^{-5}$
B (2% noise)	1.00017	0.99994	$-1.3 \times 10^{-4}$	$2.0 \times 10^{-4}$

Case	error of $a$	error of $b$	error of $c$	error of $d$	time
A (no noise)	$6.94 \times 10^{-4}$	$4.25 \times 10^{-4}$	0	0	609.30s
A (2% noise)	$2.58 \times 10^{-4}$	$1.89 \times 10^{-4}$	0	0	645.68s
B (no noise)	$6.00 \times 10^{-5}$	$1.03 \times 10^{-4}$	$4.05 \times 10^{-4}$	$5.00 \times 10^{-6}$	635.56s
B (2% noise)	$1.68 \times 10^{-4}$	$5.90 \times 10^{-5}$	$1.32 \times 10^{-4}$	$1.99 \times 10^{-5}$	637.18s

cases by considering the system

$$\begin{cases} u_t + 6u^2u_x + u_{xxx} = 0, \\ v_t + 6vv_x + v_{xxx} = 0, \\ v - iau_x - bu^2 - cuu_x - du_{xx} = 0. \end{cases} \quad (15)$$

The training data-set is generated from the known bright soliton of the focusing mKdV equation (11):

$$u = k \operatorname{sech}(kx - k^3t + x_0), \quad (16)$$

where  $k$  is a non-zero free real parameter, and  $x - 0$  is arbitrary real constant. And the corresponding complex bright soliton of the KdV equation is

$$v = k^2 \operatorname{sech}^2(kx - k^3t + x_0) - ik^2 \operatorname{sech}(kx - k^3t + x_0) \tanh(kx - k^3t + x_0) \quad (17)$$

by the complex Miura transform (9).

*Case A.*—We fix  $c = d = 0$ , and learn the two unknown parameters  $a$ ,  $b$ . The data-set is sampled in the spatio-temporal region  $(x, t) \in [-10, 10] \times [-10, 10]$ . Moreover, 10,000 sampling points will be used in the training process, and  $k = 0.8$  in this example. A 6-layer neural network with 40 neurons per layer is used to learn system (15) to fit the exact solutions of two equations. For convenience, the initial values of all free parameters are set as 1. We choose 10,000 steps Adam and 20,000 steps L-BFGS optimizations to train the considered deep learning model. Case A in Table 2 exhibits the learning parameters about  $a$ ,  $b$ , and their errors under two senses of the training data without a noise and with a 2% noise, which imply that the used deep learning method is effective. The training times are 609.30s and 645.68s,, respectively. Moreover, the errors are exhibited in Figs. 3(b1-b4) for the cases without a noise and with a 2% noise, respectively.

*Case B.*—We learn all four unknown parameters  $a$ ,  $b$ ,  $c$ ,  $d$ . We used the same deep neural network method as Case A to study this case. Case B in Table 2 displays the learning parameters about  $a$ ,  $b$ ,  $c$ ,  $d$ , and their errors under two senses of the training data without a noise and with a 2% noise, which imply that the used deep

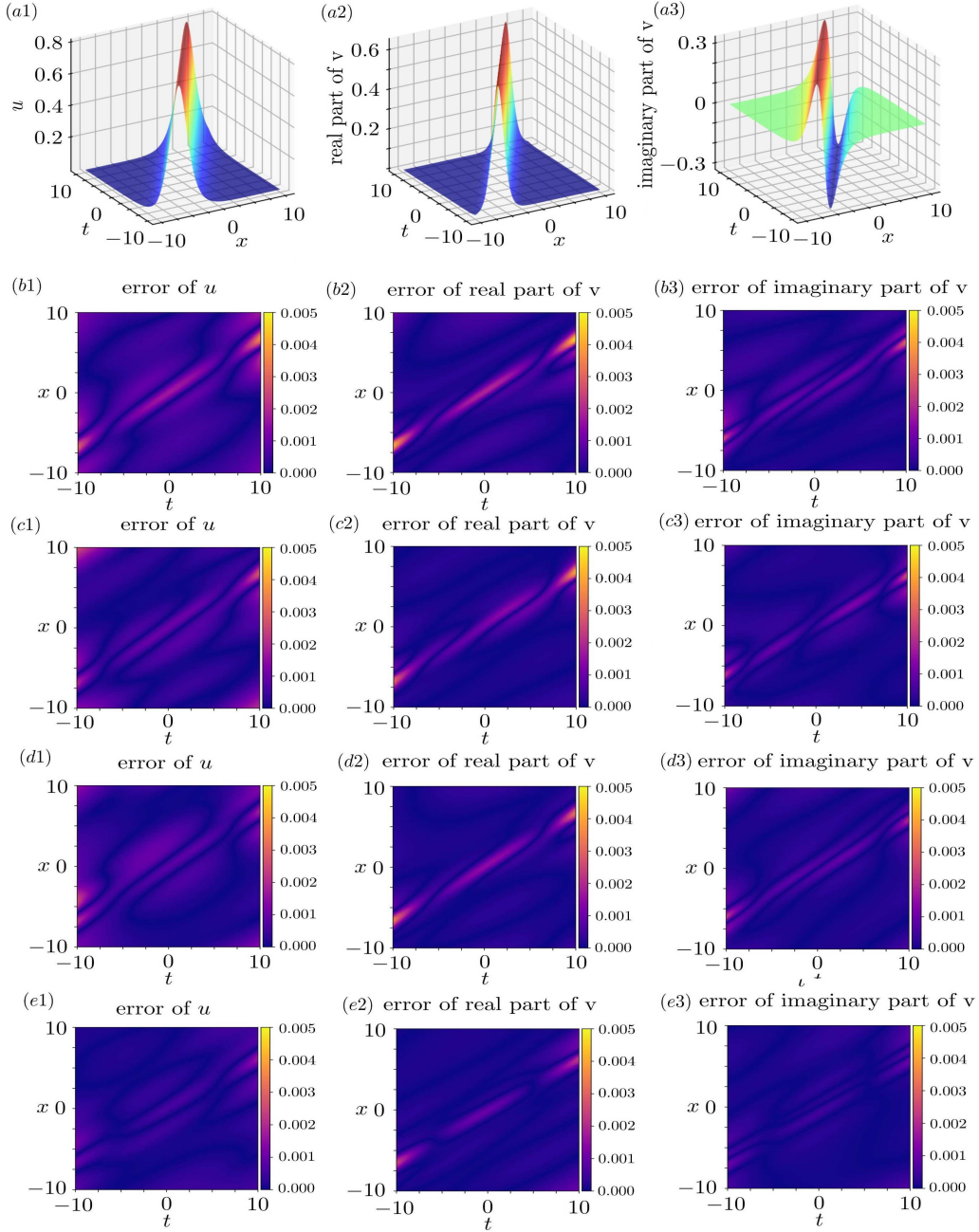


Figure 3: Data-driven complex Miura transform discovery. (a1) soliton (16), (a2, a3) real and imaginary parts of soliton (17). (b1-e3) Relative errors between exact solutions and neural network solutions: (b1-b3) Case A without a noise, (c1-c3) Case A with a 2% noise, (d1-d3) Case B without a noise, (e1-e3) Case B with a 2% noise. The relative  $L^2$ -norm errors of  $u(x, t)$ ,  $\text{Re}(v(x, t))$  and  $\text{Im}(v(x, t))$  are (b1)  $2.11\text{e-}3$ , (b2)  $2.71\text{e-}3$ , (b3)  $2.68\text{e-}3$ , (c1)  $1.69\text{e-}3$ , (c2)  $2.17\text{e-}3$ , (c3)  $2.16\text{e-}3$ , (d1)  $1.58\text{e-}3$ , (d2)  $2.00\text{e-}3$ , (d3)  $2.17\text{e-}3$ , (e1)  $9.43\text{e-}3$ , (e2)  $1.53\text{e-}3$ , and (e3)  $1.43\text{e-}3$ , respectively.

learning method is effective. The training times are 635.56s and 637.18s, respectively. Moreover, the errors are

Table 3: Data-driven discovery of real Miura transform (18) via system (19):  $a, b, c, d$  and their errors, as well as the training times.

Case	$a$	$b$	$c$	$d$	
Exact	1	-1	0	0	
Case A (no noise)	0.99999	-1.00000	0	0	
Case A (2% noise)	1.00026	-1.00012	0	0	
Case B (no noise)	1.00000	-0.99999	0.00011	-0.00013	
Case B (2% noise)	1.00019	-1.00023	0.00271	-0.00303	

Case	error of $a$	error of $b$	error of $c$	error of $d$	time
Case A (no noise)	$1.36 \times 10^{-5}$	$1.35 \times 10^{-6}$	0	0	374.40s
Case A (2% noise)	$2.55 \times 10^{-4}$	$1.22 \times 10^{-4}$	0	0	407.44s
Case B (no noise)	$7.39 \times 10^{-6}$	$5.66 \times 10^{-6}$	$1.14 \times 10^{-4}$	$1.25 \times 10^{-4}$	405.32s
Case B (2% noise)	$1.85 \times 10^{-4}$	$2.31 \times 10^{-5}$	$2.71 \times 10^{-3}$	$3.03 \times 10^{-3}$	417.00s

exhibited in Figs. 3(c1-c4) for the cases without a noise and with a 2% noise, respectively.

### Case 2. Data-driven discovery of the real Miura transform

We consider the generalized form of the real Miura transform (10) as

$$v = au_x + bu^2 + cuu_x + du_{xx}. \quad (18)$$

where  $a, b, c, d$  are four real parameters to be determined. If  $a = b = 1, c = d = 0$ , then the transform (18) reduces to the known real Miura transform (10).

In what follows, we would like to use the above-mentioned deep leaning scheme to discover these parameters  $a, b, c, d$  of the Miura transform (18) between the mKdV equation and KdV equation in two cases by considering the system

$$\begin{cases} u_t - 6u^2u_x + u_{xxx} = 0, \\ v_t + 6vv_x + v_{xxx} = 0, \\ v - au_x - bu^2 - cuu_x - du_{xx} = 0. \end{cases} \quad (19)$$

The training data-set is obtained through a shock wave solution of the defocusing mKdV equation (12)

$$u(x, t) = k \tanh(kx + k^3t) \quad (20)$$

with a free real parameter  $k \neq 0$ , and the soliton solution of the KdV equation (13)

$$v(x, t) = 2k^2 \operatorname{sech}^2(kx + 2k^3t) - k^2 \quad (21)$$

via the real Miura transform (10).

*Case A.*—We fix  $c = d = 0$ , and learn the two parameters  $a, b$ . The data-set is sampled in the spatio-temporal region  $(x, t) \in [-3, 3] \times [-3, 3]$ . Moreover, 10,000 sampling points will be used in the training process, and  $k = 1$  in this example. A 7-layer neural network with 20 neurons per layer is used to learn system (19) to fit the exact

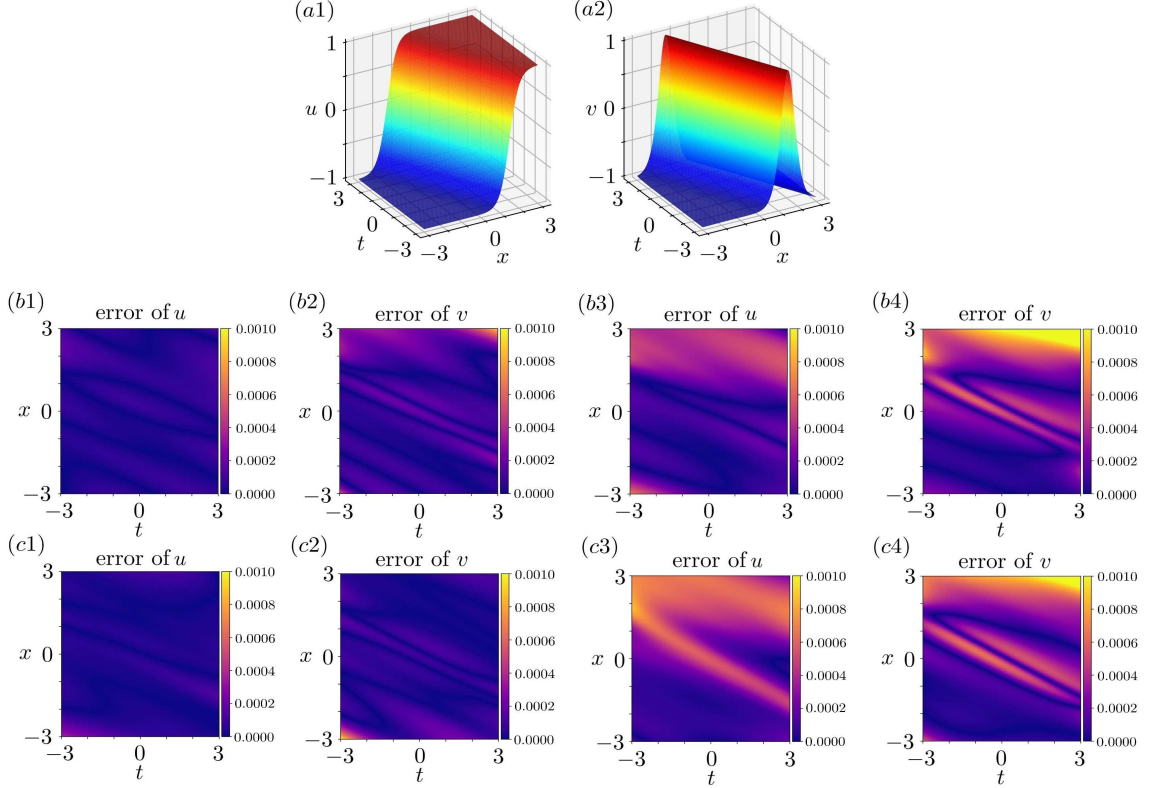


Figure 4: Data-driven discovery of real Miura transform. (a1) solution(20),(a2) soliton solution(21). (b1-e4) Relative errors between exact solutions and neural network solutions: (b1-b2) Case A without a noise, (b3-b4) Case A with a 2% noise,(c1-c2) Case B without a noise, (c3-c4) Case B with a 2% noise. The relative  $\mathbb{L}^2$ -norm errors of  $u(x, t)$  and  $v(x, t)$  are (b1)  $5.74e-5$ , (b2)  $1.44e-4$ , (b3)  $2.69e-4$ , (b4)  $4.42e-4$ , (c1)  $5.37e-5$ , (c2)  $9.37e-5$ , (c3)  $4.17e-4$ , and (c4)  $3.91e-4$ , respectively.

solutions of two equations. For convenience, the initial value of all free parameters are set as 1. We choose 5,000 steps Adam and 5,000 steps L-BFGS optimizations to train the considered deep learning model. Case A in Table 3 exhibits the learning parameters about  $a$ ,  $b$ , and their errors under two senses of the training data without a noise and with a 2% noise, which imply that the used deep learning method is effective. The training times are 374.40s and 407.44s, respectively. Moreover, the errors are exhibited in Figs. 4(b1-c3) for the cases without a noise and with a 2% noise, respectively.

*Case B.*—We learn all four parameters  $a$ ,  $b$ ,  $c$ ,  $d$ . We used the same deep neural network method as Case A to study this case. Case B in Table 3 displays the learning parameters about  $a$ ,  $b$ ,  $c$ ,  $d$ , and their errors under two senses of the training data without a noise and with a 2% noise, which imply that the used deep learning method is effective. The training times are 405.32s and 417.00s, respectively. Moreover, the errors are exhibited in Figs. 4(d1-e3) for the cases without a noise and with a 2% noise, respectively.

### 2.3 Data-driven discoveries of mKdV equations via Miura transforms

In the following we will use the known complex Miura transform (9) or real Miura transform (10) and the corresponding known solution (17) or (21) of the KdV equation (13) to discover the unknown mKdV equation

given by Eq. (22) by using the above deep learning scheme.

### 2.3.1 Data-driven discovery of the focusing mKdV equation via the complex Miura transform

In this subsection, we would like to use the above-mentioned deep learning scheme to learn the mKdV equation through the complex Miura transform (9). The solution  $u$  of the focusing mKdV equation (11) can not be explicitly expressed by the solution  $v$  of the KdV equation (13). The training data-set of  $u$  can not be directly calculated by the data-set of  $v$ . So, we will use a neural network to approximate  $u$  directly. Training the loss  $TL_T$  brings  $u$  close to the right solution.

We would like to consider the generalized form of the original mKdV equation (11)

$$u_t + au^2u_x + bu_{xxx} + cuu_{xx} + du^4 = 0 \quad (22)$$

to test the robustness of our scheme, where  $a, b, c, d$  are real-valued parameters to be determined.

We use the above-mentioned deep learning scheme to discover the parameters of the mKdV equation (22) via the complex Miura transform (9) and KdV equation (13) in two cases by considering the system

$$\begin{cases} u_t + au^2u_x + bu_{xxx} + cuu_{xx} + du^4 = 0, \\ v - iu_x - u^2 = 0. \end{cases} \quad (23)$$

*Case A.*—We fix  $c = d = 0$ , and learn the two parameters  $a, b$ . The training data-set is generated by the soliton (17) of the KdV equation. The data-set is sampled in the spatio-temporal region  $(x, t) \in [-10, 10] \times [-5, 5]$ . Moreover, 10,000 sampling points will be used in the training process, and  $k = 0.8$  in this example. A 6-layer neural network with 40 neurons per layer is used to learn system (23) to fit the exact solutions of two equations. For convenience, the initial values of all free parameters are chosen as 1. We choose 10,000 steps Adam and 20,000 steps L-BFGS optimizations to train the considered deep learning model. Case A in Table 4 exhibits the learning parameters about  $a, b$ , and their errors under two senses of the training data without a noise and with a 2% noise, which imply that the used deep learning method is effective. The training times are 768.54s and 764.55s, respectively. Moreover, the errors are exhibited in Figs. 5(b1-b4) for the cases without a noise and with a 2% noise, respectively.

*Case B.*—We learn all four parameters  $a, b, c, d$ . We used the same deep neural network method as Case A to study this case. Case B in Table 4 displays the learning parameters about  $a, b, c, d$ , and their errors under two senses of the training data without a noise and with a 2% noise, which imply that the used deep learning method is effective. The training times are 742.11s and 750.01s, respectively. Moreover, the errors are exhibited in Figs. 5(c1-c4) for the cases without a noise and with a 2% noise, respectively.

### 2.3.2 Data-driven discovery of the defocusing mKdV equation via the real Miura transform

In this subsection, we would like to train the defocusing mKdV equation through the real Miura transform (10). In general, the solution  $u$  of the defocusing mKdV equation (12) is very difficultly expressed by the solution  $v$  of the KdV equation (13). The training data of  $u$  can not be directly generated by the data-set of  $v$ . So, we will use a neural network to approximate  $u$  directly. The smaller training loss  $TL_T$  can make the trained  $\hat{u}$  close to real solution  $u$ .

We would like to consider the generalized form of the original mKdV equation given by Eq. (22) to test the robustness of our scheme. We use the above-mentioned deep learning scheme to discover the parameters of the mKdV equation (22) via the real Miura transform (10) and KdV equation (13) in two cases by considering the system

$$\begin{cases} u_t + au^2u_x + bu_{xxx} + cuu_{xx} + du^4 = 0, \\ v - u_x + u^2 = 0. \end{cases} \quad (24)$$

Table 4: Data-driven discovery of the focusing mKdV equation (22) via system (23) with the complex Miura transform (9):  $a, b, c, d$ , and their errors, as well as the training times.

Case	$a$	$b$	$c$	$d$
Exact	6	1	0	0
A (no noise)	5.94175	0.98650	0	0
A (2% noise)	5.90499	0.97883	0	0
B (no noise)	5.96718	0.99260	$1.88 \times 10^{-3}$	$1.37 \times 10^{-3}$
B (2% noise)	5.95149	0.98922	$3.3 \times 10^{-4}$	$-3.8 \times 10^{-4}$

Case	error of $a$	error of $b$	error of $c$	error of $d$	time
A (no noise)	$5.83 \times 10^{-2}$	$1.35 \times 10^{-2}$	0	0	768.54s
A (2% noise)	$9.50 \times 10^{-2}$	$2.12 \times 10^{-2}$	0	0	764.55s
B (no noise)	$3.28 \times 10^{-2}$	$7.40 \times 10^{-3}$	$1.88 \times 10^{-3}$	$1.37 \times 10^{-3}$	742.11s
B (2% noise)	$4.85 \times 10^{-2}$	$1.08 \times 10^{-2}$	$3.27 \times 10^{-4}$	$3.80 \times 10^{-4}$	750.01s

*Case A.*—We fix  $c = d = 0$ , and learn the two unknown parameters  $a, b$ . The training data-set is generated by the soliton (21) of the KdV equation. The data-set is sampled in the spatio-temporal region  $(x, t) \in [-3, 3] \times [-3, 3]$ . Moreover, 10,000 sampling points will be used in the training process, and  $k = 0.8$  in this example. A 7-layer neural network with 20 neurons per layer is used to learn system (24) to fit the exact solutions of two equations. For convenience, the initial value of all free parameters are set as 1. We choose 5,000 steps Adam and 5,000 steps L-BFGS optimizations to train the considered deep learning model. Case A in Table 5 exhibits the learning parameters about  $a, b$ , and their errors under two senses of the training data without a noise and with a 2% noise, which imply that the used deep learning method is effective. The training times are 203.41s and 178.44s, respectively. Moreover, the errors are exhibited in Figs. 6(b1, b2) for the cases without a noise and with a 2% noise, respectively.

*Case B.*—We learn all four unknown parameters  $a, b, c, d$ . We used the same deep neural network method as Case A to study this case. Case B in Table 5 displays the learning parameters about  $a, b, c, d$ , and their errors under two senses of the training data without a noise and with a 2% noise, which imply that the used deep learning method is effective. The training times are 178.08s and 163.98s, respectively. Moreover, the errors are exhibited in Figs. 6(b3, b4) for the cases without a noise and with a 2% noise, respectively.

### 3 The BT-enhanced scheme for the data-driven PDE discovery

Some deep learning schemes about the PDE discovery usually only used the basic physical data (e.g., PDE solution data) and the possible forms of the presupposed PDEs (see, e.g., Ref. [39]). Sometime they are not effective. In this section, we will propose an enhanced scheme of PDE discovery based on the BTs. We can consider the BTs into two forms, including implicit and explicit forms, to learn the soliton equations.

#### 3.1 The BT-enhanced deep learning scheme for the PDE discovery

In this section, we will provide the framework of our scheme. The main idea about the PDE discovery in the previous works is to use the solution information, which may be generated by the experimental data-set or given

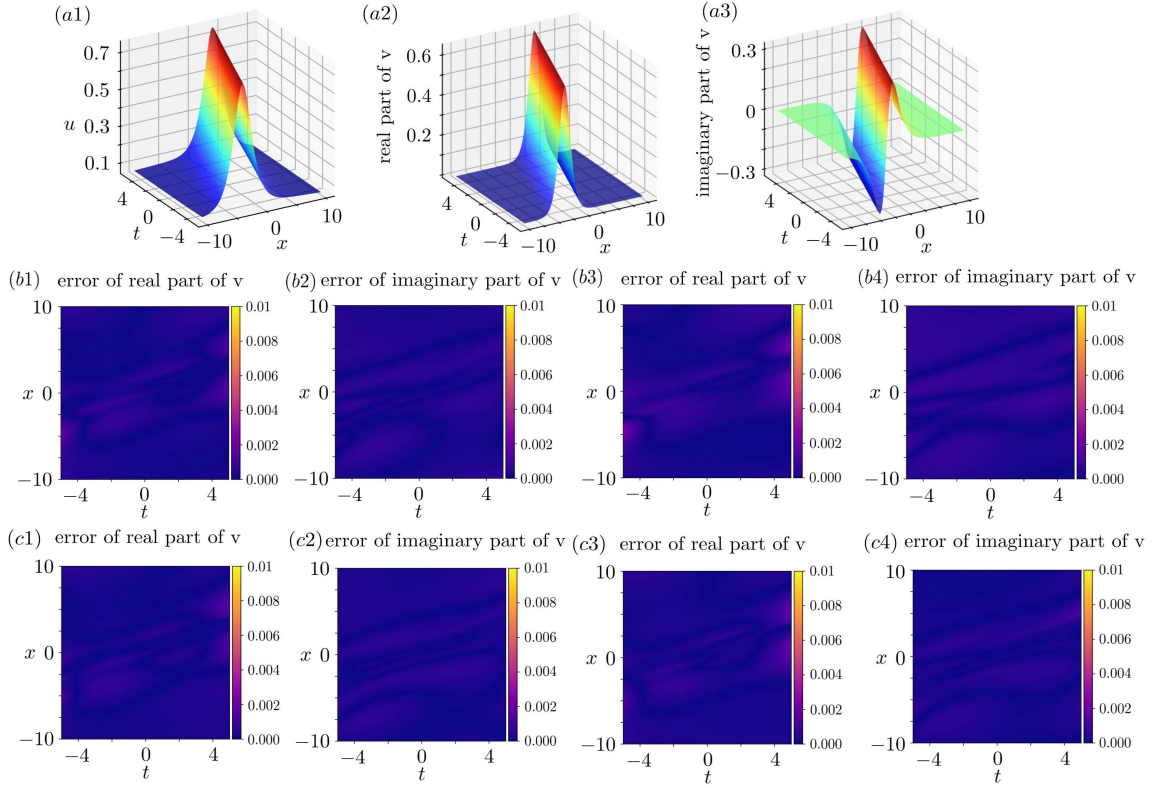


Figure 5: Data-driven discovery of the focusing mKdV equation via the complex Miura transform. (a1) trained soliton of mKdV equation, (a2-a3) real and imaginary parts of trained soliton of the KdV equation. (b1, b2) Case A without a nose, (b3, b4) Case A with a 2% noise, (c1, c2) Case B without a noise, (c3, c4) Case B with a 2% noise. The relative  $\mathbb{L}^2$ -norm errors of  $\text{Re}(v(x, t))$  and  $\text{Im}(v(x, t))$  are (b1)  $1.66 \times 10^{-3}$ , (b2)  $2.30 \times 10^{-3}$ , (b3)  $2.26 \times 10^{-3}$ , (b4)  $3.27 \times 10^{-3}$ , (c1)  $1.49 \times 10^{-3}$ , (c2)  $2.03 \times 10^{-3}$ , (c3)  $1.68 \times 10^{-3}$ , and (c4)  $1.92 \times 10^{-3}$ , respectively.

one. But if we know the BT of the original equation, then we can find the higher accuracies of parameters in the original equation. The basic idea of this method is to add the high-order constraints generated by the BTs to the training process.

We will discuss our scheme in the two different cases. In the first case, the BT can be written as an explicit form. In the second case, the BT can be given only in an implicit form.

*Case 1.*—Fig 7 exhibits the case that the BT can be written as an explicit form.  $\hat{u}_0(x, t)$  and  $\hat{u}_1(x, t)$  are represented by some neural networks, such as the fully-connected neural networks or other kinds of neural networks. The data-set  $\{u_0(x_j, t_j)\}_{j=1}^{N_p}$  arises from the experimental data or solution data. And the first-order data-set  $\{u_1(x_j, t_j)\}_{j=1}^{N_p}$  is only calculated from the above data-set  $\{u_0(x_j, t_j)\}_{j=1}^{N_p}$  by some BT. The unknown equations contain some parameters to be learned. The train loss contains the three parts:  $\text{TL}_{u_0}$ ,  $\text{TL}_{BT}$  and  $\text{TL}_F$ , where  $\text{TL}_{u_0}$  and  $\text{TL}_{u_1}$  make the neural network model fit the data-set, and the  $\text{TL}_F$  makes the unknown equation approach the exact form, which composed by the above neural network solution. If necessary, the high-order solutions can generate the stronger constraints. It is worth noting that the data-set  $\{u_1(x_j, t_j)\}_{j=1}^{N_p}$  should be prepared before the training.

Table 5: Data-driven defocusing mKdV equation (22) discovery via system (24) with the real Miura transform (10):  $a, b, c, d$ , and their errors, as well as the training times.

Case	$a$	$b$	$c$	$d$
Exact	-6	1	0	0
Case A (no noise)	-5.98709	0.99742	0	0
Case A (2% noise)	-5.97933	0.99527	0	0
Case B (no noise)	-5.98739	0.99681	-0.00330	-0.00122
Case B (2% noise)	-5.97631	0.99433	-0.00204	-0.00149

Case	error of $a$	error of $b$	error of $c$	error of $d$	time
Case A (no noise)	$1.29 \times 10^{-2}$	$2.58 \times 10^{-3}$	0	0	203.41s
Case A (2% noise)	$2.07 \times 10^{-2}$	$4.73 \times 10^{-3}$	0	0	178.44s
Case B (no noise)	$1.26 \times 10^{-2}$	$3.19 \times 10^{-3}$	$3.30 \times 10^{-3}$	$1.22 \times 10^{-3}$	178.08s
Case B (2% noise)	$2.37 \times 10^{-2}$	$5.67 \times 10^{-3}$	$2.04 \times 10^{-3}$	$1.50 \times 10^{-3}$	163.98s

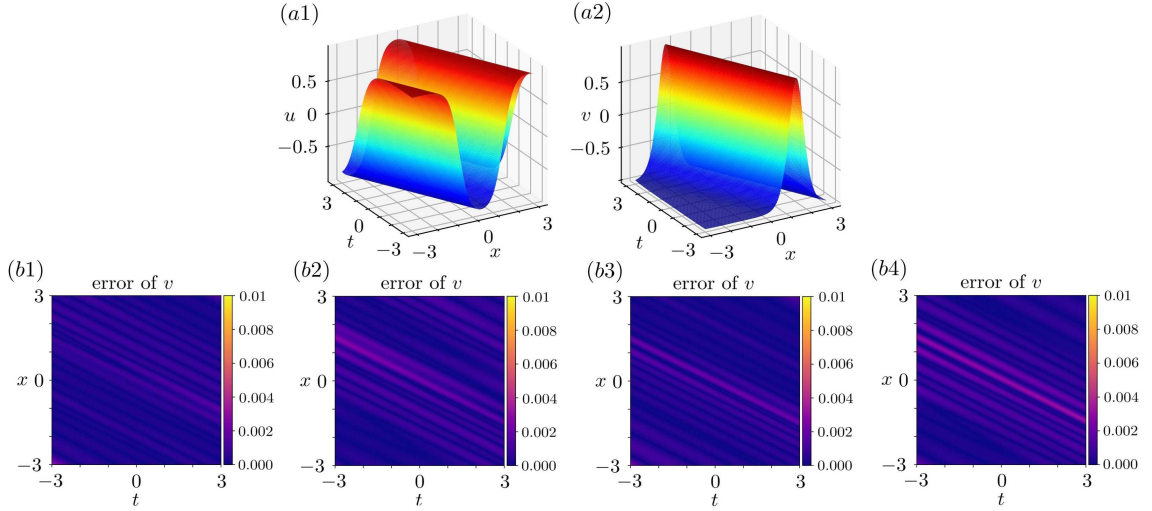


Figure 6: Data-driven discovery of the defocusing mKdV equation via the real Miura transform. (a1) trained soliton of mKdV equation, (a2) trained soliton of the KdV equation. (b1) Case A without a nose, (b2) Case A with a 2% noise, (b3) Case B without a noise, (b4) Case B with a 2% noise. The relative  $\mathbb{L}^2$ -norm errors of  $v(x, t)$  are (b1) $5.44 \times 10^{-4}$ , (b2) $8.25 \times 10^{-4}$ , (b3) $6.19 \times 10^{-4}$ , and (b4) $9.64 \times 10^{-4}$ , respectively.

The train loss is given by  $\text{TL} = \text{TL}_{u_0} + \text{TL}_{BT} + \text{TL}_F$ , where

$$\text{TL}_{u_0} = \frac{1}{N_p} \sum_{j=1}^{N_p} |u_0(x_j, t_j) - \hat{u}_0(x_j, t_j)|^2, \quad (25)$$

$$\text{TL}_{BT} = \frac{1}{N_p} \sum_{j=1}^{N_p} |BT(u_0(x_j, t_j)) - \hat{u}_1(x_j, t_j)|^2, \quad (26)$$

$$\text{TL}_F = \frac{1}{N_p} \sum_{j=1}^{N_p} \left( |F(\hat{u}_0(x_j, t_j))|^2 + |F(\hat{u}_1(x_j, t_j))|^2 \right), \quad (27)$$

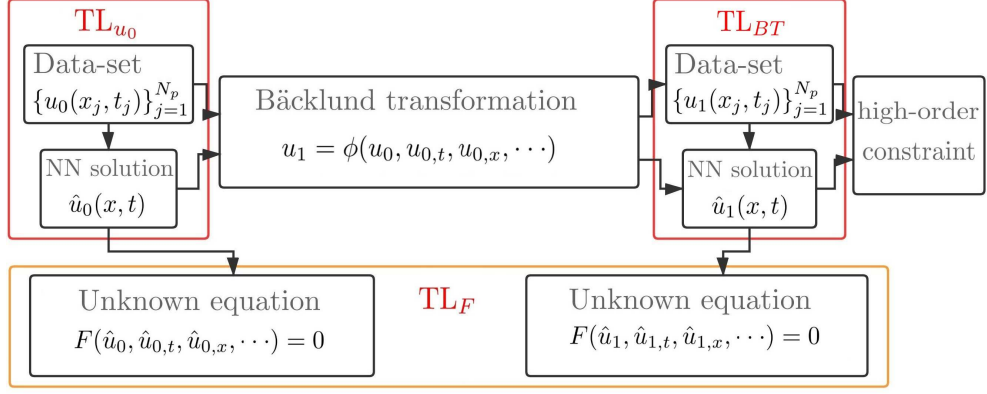


Figure 7: The BT-enhanced PDE discovery scheme for the explicit BTs.

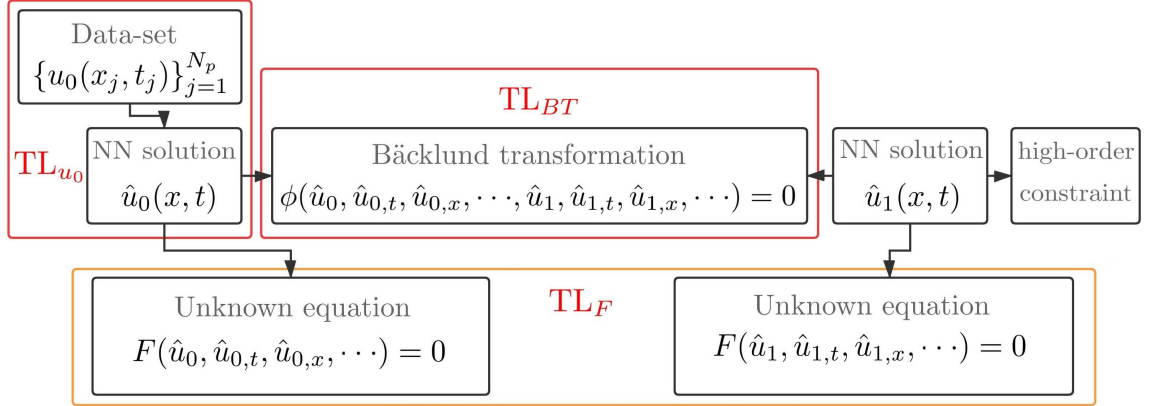


Figure 8: The BT-enhanced PDE discovery scheme for the implicit BTs.

in which  $TL_{u_0}$  and  $TL_{BT}$  make the neural network model fit the data-set,  $TL_F$  makes the unknown equation approach to the exact form, which composed by above neural network solutions  $\hat{u}_0$  and  $\hat{u}_1$ . If necessary, high-order solution can be used to obtain the stronger constraints. For instance, if we use  $\{u_0(x_j, t_j)\}_{j=1}^{N_p}$ ,  $\{BT(u_0(x_j, t_j))\}_{j=1}^{N_p}$  and 2-order data-set  $\{BT^2(u_0(x_j, t_j))\}_{j=1}^{N_p}$  to train our model to obtain the neural network solutions  $\hat{u}_j$  ( $j = 0, 1, 2$ ). The losses  $TL_{BT}$  and  $TL_F$  in the TL are replaced by

$$TL_{BT^2} = \frac{1}{N_p} \sum_{j=1}^{N_p} \left( |BT(u_0(x_j, t_j)) - \hat{u}_1(x_j, t_j)|^2 + |BT^2(u_0(x_j, t_j)) - \hat{u}_2(x_j, t_j)|^2 \right), \quad (28)$$

$$TL_F = \frac{1}{N_p} \sum_{j=1}^{N_p} \left( |F(\hat{u}_0(x_j, t_j))|^2 + |F(\hat{u}_1(x_j, t_j))|^2 + |F(\hat{u}_2(x_j, t_j))|^2 \right). \quad (29)$$

*Case 2.*—Fig 8 displays the case that the BT can be written as an implicit form. Since the BT is an implicit form, thus we can not get the data-set of  $u_1(x, t)$ . We use the training loss  $TL_{BT}$  to obtain the approximated

neural network solution  $\hat{u}_1(x, t)$ . And the approximated neural network solution  $\hat{u}_0(x, t)$  can still be trained by the data-set  $\{u_0(x_j, t_j)\}_{j=1}^{N_p}$  through  $\text{TL}_{u_0}$ . The unknown equation will be learned by  $\text{TL}_F$ . The correct equation will be found more precise by the above two schemes. These models are trained by the efficient Adam optimization algorithm and L-BFGS optimization algorithm.

The loss function of this scheme is

$$\text{TL} = \text{TL}_{u_0} + \text{TL}_{BT} + \text{TL}_F, \quad (30)$$

where

$$\text{TL}_{u_0} = \frac{1}{N_p} \sum_{j=1}^{N_p} |u_0(x_j, t_j) - \hat{u}_0(x_j, t_j)|^2, \quad (31)$$

$$\text{TL}_{BT} = \frac{1}{N_p} \sum_{j=1}^{N_p} |\phi(\hat{u}_0(x_j, t_j), \hat{u}_1(x_j, t_j))|^2, \quad (32)$$

$$\text{TL}_F = \frac{1}{N_p} \sum_{j=1}^{N_p} \left( |F(\hat{u}_0(x_j, t_j))|^2 + |F(\hat{u}_1(x_j, t_j))|^2 \right). \quad (33)$$

The exact equation will be found more precise by the above scheme. If one wants to obtain the higher accuracies of unknown equations, an additional neural network solution  $\hat{u}_2$  should be added. The losses  $\text{TL}_{BT}$  and  $\text{TL}_F$  in the TL are replaced by

$$\text{TL}_{BT^2} = \frac{1}{N_p} \sum_{j=1}^{N_p} \left( |\phi(\hat{u}_0(x_j, t_j), \hat{u}_1(x_j, t_j))|^2 + |\phi(\hat{u}_1(x_j, t_j), \hat{u}_2(x_j, t_j))|^2 \right) \quad (34)$$

and

$$\text{TL}_F = \frac{1}{N_p} \sum_{j=1}^{N_p} \left( |F(\hat{u}_0(x_j, t_j))|^2 + |F(\hat{u}_1(x_j, t_j))|^2 + |F(\hat{u}_2(x_j, t_j))|^2 \right). \quad (35)$$

In the two above schemes, if we only use  $\hat{u}_0$  and  $\hat{u}_1$  to train the neural network, then we call it the 1-fold BT-enhanced (BTE) scheme. And if we use  $\hat{u}_0$ ,  $\hat{u}_1$  and  $\hat{u}_2$  in the training process, we call it the 2-fold BTE scheme. All schemes are trained by the efficient Adam and L-BFGS optimization algorithms.

In what follows, we will display two examples to show the validity of our schemes. The first example is to learn the mKdV equation based on the explicit BT (alias Darboux transform (DT)) of the mKdV equation given by Eq. (36). The second example is to study the s-G equation via the implicit aBT (5).

### 3.2 Data-driven discovery of mKdV equation via the explicit BT/DT

Here we would like to use the known solution  $u_1$ , and the explicit BT/DT (36) generating the new solution  $u_2$  from  $u_1$  to discover the unknown mKdV equation (40) with some perturbation terms via the BT-enhanced scheme.

The focusing mKdV equation (11) possesses the BT/DT [60]

$$u_{n+1} = u_n + \frac{4\lambda\psi}{1 + \psi^2}, \quad \psi = \frac{\Phi_{22}(x, t, \lambda) + \mu\Phi_{21}(x, t, \lambda)}{\Phi_{12}(x, t, \lambda) + \mu\Phi_{11}(x, t, \lambda)} \quad (36)$$

with a free parameter  $\mu$ , where

$$\Phi = \begin{pmatrix} \Phi_{11}(x, t, \lambda) & \Phi_{12}(x, t, \lambda) \\ \Phi_{21}(x, t, \lambda) & \Phi_{22}(x, t, \lambda) \end{pmatrix}$$

Table 6: Comparisons of PINNs and BT-enhanced scheme for the data-driven mKdV equation discovery.

Case	$a$	error of $a$	$b$	error of $b$	$c$	error of $c$	$d$	error of $d$
Exact	6	0	1	0	0	0	0	0
A (PINNs)	5.63392	0.366	0.90826	0.0917	0	0	0	0
A (PINNs 2%)	5.60595	0.394	0.90041	0.0996	0	0	0	0
A (PINNs 5%)	5.56262	0.437	0.89004	0.110	0	0	0	0
A (PINNs 10%)	5.58002	0.420	0.89078	0.109	0	0	0	0
A (PINNs 20%)	3.64644	2.35356	0.45905	0.541	0	0	0	0
B (PINNs)	5.58765	0.412	0.90205	0.0979	-0.02825	0.0282	-0.01493	0.0149
B (PINNs 2%)	5.80756	0.192	0.95514	0.0449	-0.02467	0.0247	-0.02322	0.0232
B (PINNs 5%)	5.74998	0.250	0.94189	0.0581	-0.01166	0.0117	-0.01847	0.0185
B (PINNs 10%)	5.63770	0.362	0.91263	0.0874	-0.00343	0.00343	-0.01174	0.0117
B (PINNs 20%)	4.86428	1.14	0.73158	0.268	-0.02057	0.0206	-0.00608	0.00608
A (BTE)	6.00973	$9.73 \times 10^{-3}$	1.00123	$1.23 \times 10^{-3}$	0	0	0	0
A (BTE 2%)	5.97970	$2.03 \times 10^{-2}$	0.99380	$6.20 \times 10^{-3}$	0	0	0	0
A (BTE 5%)	5.98296	$1.70 \times 10^{-2}$	0.99231	$7.69 \times 10^{-3}$	0	0	0	0
A (BTE 10%)	5.99462	$5.38 \times 10^{-3}$	0.99104	$8.96 \times 10^{-3}$	0	0	0	0
A (BTE 20%)	5.97702	$2.30 \times 10^{-2}$	0.97901	$2.10 \times 10^{-2}$	0	0	0	0
B (BTE)	5.99109	$8.91 \times 10^{-3}$	0.99804	$1.96 \times 10^{-3}$	0.00086	$8.57 \times 10^{-4}$	0.00110	$1.10 \times 10^{-3}$
B (BTE 2%)	5.99943	$5.72 \times 10^{-4}$	0.99818	$1.82 \times 10^{-4}$	0.00013	$1.35 \times 10^{-4}$	0.00028	$2.80 \times 10^{-4}$
B (BTE 5%)	5.98173	$1.83 \times 10^{-2}$	0.99214	$7.86 \times 10^{-4}$	0.00024	$2.38 \times 10^{-4}$	0.00016	$1.62 \times 10^{-4}$
B (BTE 10%)	5.98347	$1.65 \times 10^{-2}$	0.98876	$1.12 \times 10^{-2}$	-0.00063	$6.26 \times 10^{-4}$	-0.00142	$1.42 \times 10^{-3}$
B (BTE 20%)	5.98058	$1.94 \times 10^{-2}$	0.97879	$2.12 \times 10^{-2}$	-0.00178	$1.78 \times 10^{-3}$	-0.00305	$3.05 \times 10^{-3}$

is the basic solution of the Lax pair of the mKdV equation (11)

$$\Phi_x = \begin{pmatrix} \lambda & u \\ -u & -\lambda \end{pmatrix} \Phi, \quad \Phi_t = \begin{pmatrix} -2\lambda(2\lambda^2 + u^2) & -2\lambda(2u\lambda + u_x) - 2u^3 - u_{xx} \\ 2\lambda(2u\lambda - u_x) + 2u^3 + u_{xx} & 2\lambda(2\lambda^2 + u^2) \end{pmatrix} \Phi \quad (37)$$

with  $\lambda \in \mathbb{C}$  being a spectral parameter, and  $u$  an initial solution of the mKdV equation (11).

By using the above DT (36) with  $u_0 = 0$ ,  $\mu = e^{2\alpha_1}$  and  $\lambda = \lambda_1$ , one can obtain the one-soliton solution of the mKdV equation (11)

$$u_1(x, t) = 2\lambda_1 \operatorname{sech}(2\lambda_1 x - 8\lambda_1^3 t + 2\alpha_1) \quad (38)$$

Further, one can use the DT (36) with  $u_1$  given by Eq. (38),  $\mu = e^{2\alpha_2}$  and  $\lambda = \lambda_2$ , to find the 2-soliton solution of the mKdV equation (11) in the form

$$u_2(x, t) = \frac{2(\lambda_2^2 - \lambda_1^2)(\lambda_2 \cosh(v_1) - \lambda_1 \cosh(v_2))}{(\lambda_1^2 + \lambda_2^2) \cosh(v_1) \cosh(v_2) - 2\lambda_1 \lambda_2 (1 + \sinh(v_1) \sinh(v_2))}, \quad (39)$$

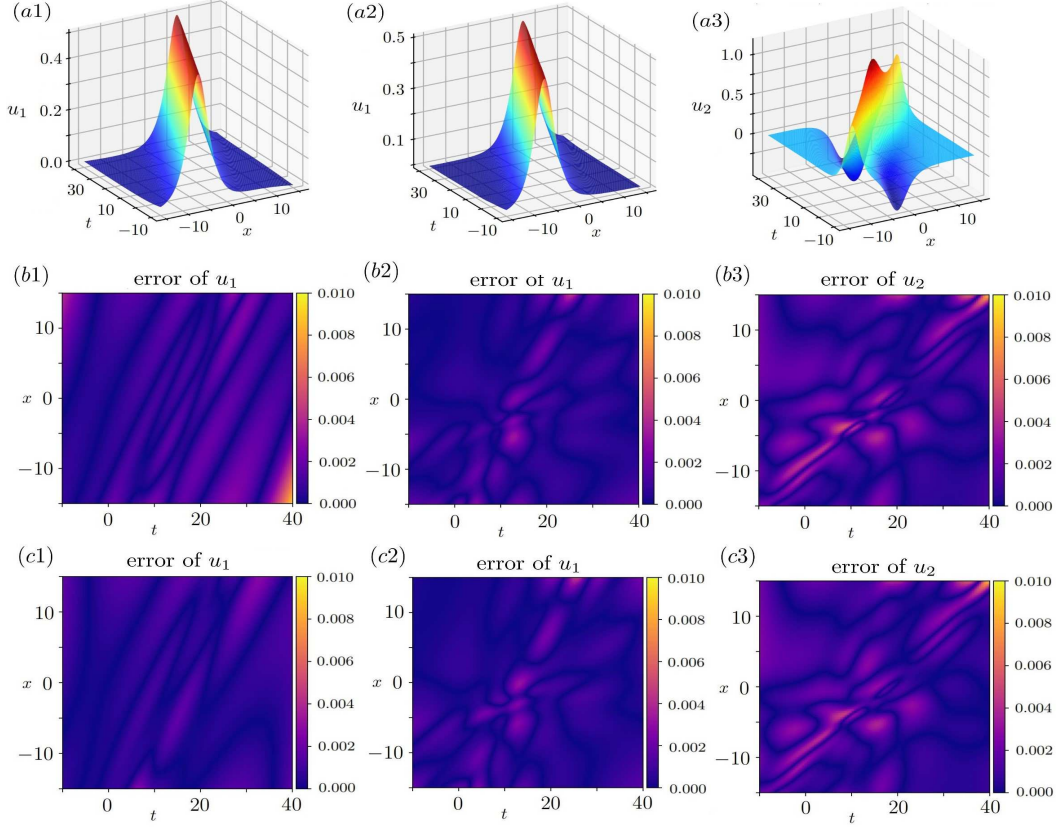


Figure 9: Focusing mKdV equation. (a1) trained one-soliton solution via PINNs and (a2, a3) trained one- and two-soliton solutions via the BT-enhanced PDE scheme. (b1-c3) absolute errors: (b1) PINNs learning Case A with a 5% noise, (b2-b3) BT-enhanced PDE scheme learning Case A with a 5% noise, (c1) PINNs learning Case B with a 5% noise, (c2-c3) BT-enhanced PDE scheme learning Case B with a 5% noise. The relative  $\mathbb{L}^2$ -norm errors of  $u_1$  and  $u_2$  are: (b1)  $6.61 \times 10^{-3}$ , (b2)  $3.71 \times 10^{-3}$ , (b3)  $4.61 \times 10^{-3}$ , (c1)  $5.81 \times 10^{-2}$ , (c2)  $3.80 \times 10^{-3}$ , and (c3)  $4.41 \times 10^{-3}$ , respectively. The training times are (b1) 132.14s, (b2-b3) 302.67s, (c1) 135.95s, and (c2-c3) 285.60s, respectively.

where  $v_j = 2\lambda_j x - 8\lambda_j^3 t + 2\alpha_j$ , ( $j = 1, 2$ ), and  $\lambda_2 > \lambda_1 > 0$ . In this example, we take  $\lambda_1 = \frac{1}{4}$ ,  $\lambda_2 = \frac{1}{3}$ ,  $\alpha_1 = 1$ , and  $\alpha_2 = 2$ . According to the homogeneity principle of the mKdV equation, we add two disturbance terms  $u^4$ ,  $uu_{xx}$  to the mKdV equation to generate the generalized form

$$u_t + au^2u_x + bu_{xxx} + cu^4 + duu_{xx} = 0, \quad (40)$$

which is used to examine the robustness of the scheme, where  $a$ ,  $b$ ,  $c$ , and  $d$  are real-valued parameters to be determined.

In what follows, we would like to use the above-mentioned BT-enhanced PDE discovery scheme given by Fig. 7 to discover these parameters  $a$ ,  $b$ ,  $c$ ,  $d$  of the mKdV equation (40) in two cases by considering the system

$$\begin{cases} u_t + au^2u_x + bu_{xxx} + cu^4 + duu_{xx} = 0, \\ u_2 - u_1 - \frac{4\lambda\psi}{1 + \psi^2} = 0. \end{cases} \quad (41)$$

The training data-set is generated by the soliton solution (38) of the focusing mKdV equation (11). To compare

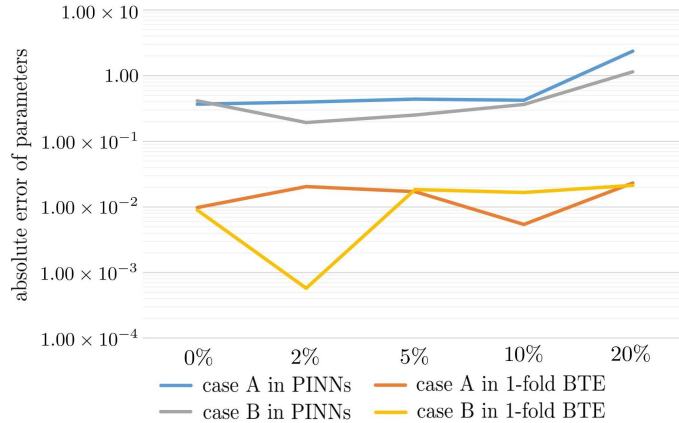


Figure 10: Error comparisons between the BTE and PINNs schemes for the mKdV equation. The vertical axis is the maximum of the absolute errors of all parameters.

our scheme with the known PINNs scheme [39], which is trained by considering Eq. (40) with the initial data generating from  $u_1$ .

*Case A.*—We fix  $c = d = 0$ , and learn two unknown parameters  $a$  and  $b$ . We take the initial values of  $a, b$  as  $a = b = 1$ . The training data-set is generated by not only the one-soliton solution (38) but also the two-soliton solution (39) of the mKdV equation. The training data-set is sampled in the region  $(x, t) \in [-15, 15] \times [-10, 40]$ , and 10,000 sampling points are used in the training processes. For the BT-enhanced PDE discovery scheme given by Fig. 7, two solitons  $u_1$  and  $u_2$  are approximated by using a 6-layer neural network with 40 neurons per layer, and 5,000 steps Adam and 5,000 steps L-BFGS optimizations are chosen. We use the usual PINNs with the training data arising from the one-soliton solution  $u_1$ , and our scheme with the same neural network to learn two parameters  $a, b$ , respectively, such that Case A of Table 6 displays the learning results and their errors under two senses of the training data without a noise and with the differential 2%, 5%, 10%, 20% noises. Figs. 9 and 10 exhibit the errors of training results of all conditions, which imply that our scheme is better than the PINNs scheme for the same training steps. That is to say, except for the one-soliton data arising from  $u_1$ , the used more data  $u_2$  generated from the DT (36) can make the errors of learning results smaller in the BT-enhanced PDE discovery scheme given by Fig. 7.

*Case B.*—We train all four unknown parameters  $a, b, c, d$  in Eq. (40). We used the same BT-enhanced PDE discovery scheme given by Fig. 7 as Case A and PINNs to study this case, respectively. For the two senses of the training data without a noise and with the differential 2%, 5%, 10%, 20% noises, Case B in Table 6 displays the learning parameters about  $a, b, c, d$ , and their errors via our scheme and the known PINNs. The results imply that the BT-enhanced PDE discovery scheme given by Fig. 7 is more effective (see Figs. 9 and 10).

### 3.3 Data-driven discovery of the s-G equation via the implicit aBT

In what follows, we would like to use the known breather solution (8) and implicit aBT (5) to discover the unknown s-G equation (42) with some perturbation terms via the BT-enhanced PDE discovery scheme.

We know that the s-G equation (4) has the aBT (5), which can be used to generate its new solution  $u'(x, t)$ . In what follows, we will utilize this aBT to find the high-precision s-G equation. Meanwhile, we will compare the results between the BT-enhanced PDE discovery scheme given by Fig. 8 and known PINNs scheme [39].

Table 7: Comparisons of PINNs and BT-enhanced PDE scheme for the data-driven s-G equation discovery.

Case	$a$	error of $a$	$b$	error of $b$
Exact	1	0	0	0
PINNs (no noise)	0.99991	$9.18 \times 10^{-5}$	-0.00002	$2.16 \times 10^{-5}$
PINNs (2% noise)	1.00051	$5.13 \times 10^{-4}$	-0.00005	$5.30 \times 10^{-5}$
PINNs (5% noise)	1.00128	$1.28 \times 10^{-3}$	0.00002	$1.58 \times 10^{-5}$
PINNs (10% noise)	1.00239	$2.39 \times 10^{-3}$	-0.00019	$1.90 \times 10^{-4}$
PINNs (20% noise)	1.00466	$4.66 \times 10^{-3}$	-0.00041	$4.13 \times 10^{-4}$
1-fold BTE (no noise)	0.99996	$4.15 \times 10^{-5}$	0.00001	$1.30 \times 10^{-5}$
1-fold BTE (2% noise)	1.00020	$1.98 \times 10^{-4}$	-0.00000	$7.21 \times 10^{-6}$
1-fold BTE (5% noise)	1.00057	$5.70 \times 10^{-4}$	-0.00003	$2.97 \times 10^{-5}$
1-fold BTE (10% noise)	1.00108	$1.07 \times 10^{-3}$	-0.00007	$6.46 \times 10^{-5}$
1-fold BTE (20% noise)	1.00218	$2.18 \times 10^{-3}$	-0.00010	$9.67 \times 10^{-5}$
2-fold BTE (no noise)	0.99984	$1.59 \times 10^{-4}$	-0.00004	$4.05 \times 10^{-5}$
2-fold BTE (2% noise)	1.00003	$3.42 \times 10^{-5}$	0.00002	$1.54 \times 10^{-5}$
2-fold BTE (5% noise)	1.00036	$3.58 \times 10^{-4}$	-0.00004	$3.72 \times 10^{-5}$
2-fold BTE (10% noise)	1.00081	$8.08 \times 10^{-4}$	-0.00001	$1.10 \times 10^{-5}$
2-fold BTE (20% noise)	1.00146	$1.46 \times 10^{-3}$	-0.00011	$1.12 \times 10^{-4}$

We consider the aBT of the generalized s-G equation

$$u_{xt} = a \sin u + b \cos u, \quad (42)$$

where  $a, b$  are parameters to be determined. As  $a = 1, b = 0$ , Eq. (42) reduces to the known aBT of the s-G equation [54].

In what follows, we would like to use the above-mentioned BT-enhanced PDE discovery scheme given by Fig. 8 to discover these parameters  $a, b$  of the generalized s-G equation (42) in two cases by considering the system

$$\begin{cases} u_{xt} - a \sin u - b \cos u = 0, \\ u'_x = u_x - 2\beta \sin\left(\frac{u + u'}{2}\right), \\ u'_t = -u_t + \frac{2}{\beta} \sin\left(\frac{u - u'}{2}\right). \end{cases} \quad (43)$$

The training data-set is generated by the breather solution (8) of the s-G equation (4). To compare our scheme with the known PINNs scheme, which is trained by considering Eq. (42) with the initial data generating from the breather solution (8).

The training data are generated by the breather solution (8). The 10,000 sampling points are selected in  $\{(x, t) | (x, t) \in [-10, 10] \times [-5, 5]\}$ . The 5,000 steps Adam and 5,000 steps L-BFGS optimizations will be used in each case. the trained solutions  $\hat{u}_0, \hat{u}_1$  and  $\hat{u}_2$  are represented by using one 6-layer neural network with 40 neurons per layer.  $\hat{u}_0$  will approach to the right solution (8), and  $\hat{u}_1, \hat{u}_2$  just are the neural network solutions. Fig. 11 displays the breather-like profiles of  $\hat{u}_0, \hat{u}_1$  and  $\hat{u}_2$ . Fig. 12 exhibits the training results of all conditions,

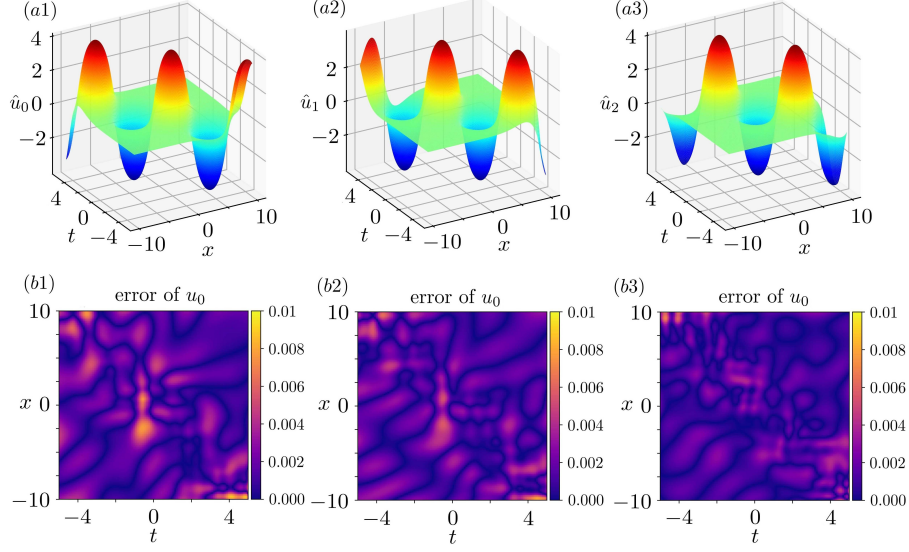


Figure 11: (a1-a3) Three neural network solutions of s-G equation via the 2-fold BTE scheme. (b1-b3) absolute errors of  $u_1$  with a 2% noise: (b1) PINNs scheme, (b2) 1-fold BTE scheme, (b3) 2-fold BTE scheme. The relative  $\mathbb{L}^2$ -norm errors of  $u_1$  and training times are (b1)  $1.51 \times 10^{-3}$ , 123.20s, (b2)  $1.33 \times 10^{-3}$ , 343.72s, (b3)  $1.01 \times 10^{-3}$ , 505.11s, respectively.

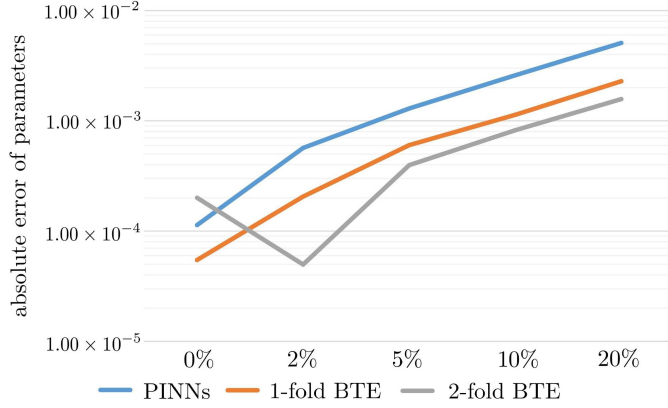


Figure 12: Error comparisons between the BTE scheme and PINNs for the sine-Gordon equation via the implicit aBT. The vertical axis is the maximum of the absolute errors of all parameters.

where the vertical axis represents the maximal errors of  $b$  and  $c$ , and the horizontal axis denotes the different error of training data. As a result, we find that our scheme is almost always better than the PINNs scheme for the same training steps.

## 4 Conclusions and discussions

In conclusion, we have established the deep neural network learning algorithms to discover the BTs and soliton evolution equations. Three types of BTs are used to investigate the availability of our schemes, such as the aBT

of the sine-Gordon equation, complex/real Miura transform between the defocusing/focusing mKdV equation and KdV equation, as well as the DT of the focusing mKdV equation. Moreover, we also compare our scheme with the known PINNs such that our scheme is more effective in the study of data-driven discoveries of soliton equations via the BTs. The idea can also be extended to other types of BTs and nonlinear evolution PDEs containing some physically interesting soliton evolution equations.

## Acknowledgements

This work was supported by the National Natural Science Foundation of China (Nos. 11925108 and 11731014).

## Data availability

All data included in this study are available upon request by contact with the corresponding author.

## Declarations

## Conflict of interest

The authors declare no conflict of interest.

## References

- [1] Korteweg, D. J., de Vries, G.: On the change of form of long waves advancing in a rectangular canal, and on a new type of long stationary waves. *Philos. Mag.* **39**, 422 (1895)
- [2] Ablowitz, M. J., Clarkson, P. A.: *Solitons, Nonlinear Evolution Equations and Inverse Scattering*. Cambridge University Press, Cambridge (1991)
- [3] Hasegawa, A., Kodama, Y.: *Solitons in Optical Communications*. Oxford University Press, Oxford (1995)
- [4] Akhmediev, N., Ankiewicz, A.: *Solitons: Nonlinear Pulses and Beams*. Chapman and Hall, London (1997)
- [5] Agrawal, G. P.: *Nonlinear Fiber Optics*. Academic Press, New York (2012)
- [6] Pitaevskii, L., Stringari, S.: *Bose-Einstein Condensation*. Oxford University Press, Oxford (2003)
- [7] Kharif, C., Pelinovsky, E., Slunyaev, A.: *Rogue Waves in the Ocean*. Springer, New York (2009)
- [8] Osborne, A.: *Nonlinear Ocean Waves and the Inverse Scattering Transform*. Elsevier, New York (2010)
- [9] Yan, Z.: Financial rogue waves. *Commun. Theor. Phys.* **54**, 947 (2010)
- [10] Yang, J.: *Nonlinear Waves in Integrable and Nonintegrable Systems*. SIAM, New York (2010)
- [11] Bäcklund, A. V.: Einiges über Curven und Flächen transformationen. *Lund Universitets Arsskrift* **10**, 1 (1875)
- [12] Darboux, G.: On a proposition relative to linear equations. *Comptes Rendus Acad. Sci.* **94**, 1456-1459 (1882)
- [13] Miura, R.: *Bäcklund Transformations*. Springer, New York (1976)
- [14] Lamb Jr, G. L.: Bäcklund transformations for certain nonlinear evolution equations. *J. Math. Phys.* **15**, 2157 (1974)
- [15] Matveev, V. B., Salle, M. A.: *Darboux Transformations and Solitons*. Springer, New York (1991)
- [16] Rogers, C., Schief, W. K.: *Bäcklund and Darboux transformations: geometry and modern applications in soliton theory*. Cambridge University Press, Cambridge (2002)
- [17] Bluman, G. W., Kumei, S.: *Symmetries and Differential Equations*. Springer, New York (1989)
- [18] Hirota, R.: *The Direct Method in Soliton Theory*. Cambridge University Press, Cambridge (2004)
- [19] Hopf, E.: The partial differential equation  $u_t + uu_x = u_{xx}$ . *Commun. Pure Appl. Math.* **3**, 201 (1950)
- [20] Cole, J. D.: On a quasi-linear parabolic equations occurring in aerodynamics. *Quart. J. Appl. Math.* **9**, 225 (1951)
- [21] Gardner, C. S., Greene, J. M., Kruskal, M. D., Miura, R. M.: Method for solving the Korteweg-de Vries equation. *Phys. Rev. Lett.* **19**, 1095 (1967)
- [22] Lax, P. D.: Integrals of nonlinear equations of evolution and solitary wave. *Commun. Pure Appl. Math.* **21**, 467 (1968)
- [23] Miura, R. M.: Korteweg-de Vries equation and generalizations. I. A remarkable explicit nonlinear transformation. *J. Math. Phys.* **9**, 1202 (1968)
- [24] Goodfellow, I., Bengio, Y., Courville, A.: *Deep learning*. MIT Press, Massachusetts (2016)
- [25] LeCun, Y., Bengio, Y., Hinton, G.: Deep learning. *Nature* **521**, 436 (2015)

- [26] Lake, B. M., Salakhutdinov, R., Tenenbaum, J. B.: Human-level concept learning through probabilistic program induction. *Science* **350**, 1332 (2015)
- [27] Krizhevsky, A., Sutskever, I., Hinton, G. E.: Imagenet classification with deep convolutional neural networks. In: Pereira, F., Burges, C. J. C., Bottou, L., Weinberger, K. Q. (eds.) *Advances in Neural Information Processing Systems*, pp. 1097-1105. Curran Associates Inc., New York (2012)
- [28] Alipanahi, B., Delong, A., Weirauch, M. T., Frey, B. J.: Predicting the sequence specificities of DNA- and RNA-binding proteins by deep learning. *Nat. Biotechnol.* **33**, 831 (2015)
- [29] Larranaga, P., Atienza, D., Diaz-Rozo, J., Ogbechie, A., Puerto-Santana, C. E., Bielza, C.: *Industrial Applications of Machine Learning*. CRC Press, Boca Raton (2019)
- [30] Johri, P., Verma, J. K., Paul, S.: (ed.) *Applications of Machine Learning*. Springer, New York (2020)
- [31] Dissanayake, M., Phan-Thien, N.: Neural-network-based approximations for solving partial differential equations. *Commun. Numer. Meth. Eng.* **10**, 195 (1994)
- [32] Lagaris, I. E., Likas, A., Fotiadis, D. I.: Artificial neural networks for solving ordinary and partial differential equations. *IEEE T. Neural Netw.* **9**, 987 (1998)
- [33] Lagaris, I. E., Likas, A. C., Papageorgiou, G. D.: Neural-network methods for boundary value problems with irregular boundaries. *IEEE T. Neural Netw.* **11**, 1041 (2000)
- [34] Rudy, S. H., Brunton, S. L., Proctor, J. L., Kutz, J. N.: Data-driven discovery of partial differential equations. *Sci. Adv.* **3**, e1602614 (2017)
- [35] Sirignano, J., Spiliopoulos, K.: DGM: A deep learning algorithm for solving partial differential equations. *J. Comput. Phys.* **375**, 1339 (2018)
- [36] Han, J., Jentzen, A., E, W.: Solving high-dimensional partial differential equations using deep learning. *PNAS* **115**, 8505 (2018)
- [37] Bar-Sinai, Y., Hoyer, S., Hickey, J., Brenner, M. P.: Learning data-driven discretizations for partial differential equations. *PNAS* **116**, 15344 (2019)
- [38] Raissi, M., Karniadakis, G. E.: Hidden physics models: machine learning of nonlinear partial differential equations. *J. Comput. Phys.* **357**, 125 (2018)
- [39] Raissi, M., Perdikaris, P., Karniadakis, G. E.: Physics-informed neural networks: A deep learning framework for solving forward and inverse problems involving nonlinear partial differential equations. *J. Comput. Phys.* **378**, 686 (2019)
- [40] M. Raissi, A. Yazdani, and G. E. Karniadakis, Hidden fluid mechanics: Learning velocity and pressure fields from flow visualizations, *Science* 367 (2020) 1026-1030.
- [41] Lu, L, Meng, X., Mao, Z., Karniadakis, G. E.: DeepXDE: A deep learning library for solving differential equations. *SIAM Rev.* **63**, 208 (2021)
- [42] Mao, Z., Jagtap, A. D., Karniadakis, G. E.: Physics-informed neural networks for high-speed flows. *Comput. Meth. Appl. Mech. Eng.* **360**, 112789 (2020)
- [43] Zhou, Z., Yan, Z.: Solving forward and inverse problems of the logarithmic nonlinear Schrödinger equation with PT-symmetric harmonic potential via deep learning. *Phys. Lett. A* **387**, 127010 (2021)
- [44] Wang, L., Yan, Z.: Data-driven rogue waves and parameter discovery in the defocusing NLS equation with a potential using the PINN deep learning. *Phys. Lett. A* **404**, 127408 (2021)
- [45] Wang, L., Yan, Z.: Data-driven peakon and periodic peakon travelling wave solutions of some nonlinear dispersive equations via deep learning. *Physica D* **428**, 133037 (2021)
- [46] Zhou, Z., Yan, Z.: Deep learning neural networks for the third-order nonlinear Schrödinger equation: Bright solitons, breathers, and rogue waves. *Commun. Theor. Phys.* **73**, 105006 (2021)
- [47] Pu, J., Li, J., Chen, Y.: Solving localized wave solutions of the derivative nonlinear Schrödinger equation using an improved PINN method. *Nonlinear Dyn* **105**, 1723-1739 (2021)
- [48] Li, J., Chen, J., Li, B.: Gradient-optimized physics-informed neural networks (GOPINNs): a deep learning method for solving the complex modified KdV equation. *Nonlinear Dyn* **107**, 781-792 (2022)
- [49] Pang, G., Lu, L., Karniadakis, G. E.: fPINNs: Fractional physics-informed neural networks. *SIAM J. Sci. Comput.* **41**, A2603 (2019)
- [50] Zhang, G., Guo, L., Karniadakis, G. E.: Learning in modal space: Solving time-dependent stochastic pdes using physics-informed neural networks. *SIAM J. Sci. Comput.* **42**, A639 (2020)
- [51] Stein, M.: Large sample properties of simulations using Latin hypercube sampling. *Technometrics* **29**, 143 (1987)
- [52] Kingma, D., Ba, J.: Adam: a method for stochastic optimization. <https://arxiv.org/abs/1412.6980> (2014)

- [53] Liu, D. C., Nocedal, J.: On the limited memory BFGS method for large scale optimization. *Math. Program.* **45**, 503 (1989)
- [54] Frenkel, J., Kontorova, T.: On the theory of plastic deformation and twinning. *J. Phys. USSR* **1**, 137 (1939)
- [55] Rubinstein, J.: Sine-Gordon equation. *J. Math. Phys.* **11**, 258 (1970)
- [56] Barone, A., Esposito, F., Magee, C. J., Scott, A. C.: Theory and applications of the sine-Gordon equation. *Riv. Nuovo Cimento* **1**, 227 (1971)
- [57] Caudrey, P. J., Eilbeck, J. C, Gibbon, J. D.: The sine-Gordon equation as a model classical field theory. *Nuovo Cimento B* **25** 497 (1975)
- [58] Miura, R.: The Korteweg-de Vries equation: A survey of results. *SIAM Rev.* **18**, 412 (1976)
- [59] Schamel, H.: A modified Korteweg-de Vries equation for ion acoustic waves due to resonant electrons. *J. Plasma Phys.* **9** 377 (1973)
- [60] Gu, C., Hu, H., Zhou, Z.: *Darboux Transformations in Integrable Systems*. Springer, New York (2005)